Online-Journals.org

iJOE International Journal of Online and Biomedical Engineering

iJOE | eISSN: 2626-8493 | Vol. 21 No. 9 (2025) | OPEN ACCESS

https://doi.org/10.3991/ijoe.v21i09.55513

PAPER

Design and Development of a 3D-Printed Tissue Equivalent Phantom for Cobalt-60 HDR Brachytherapy

Nurul Qomariyah[1], Abdul Waris[1], Rahadi Wirawan[2], Heru Prasetio[3], Freddy Haryanto[1](✉)

[1]Department of Physics, Faculty of Mathematics and Natural Science, Institut Teknologi Bandung, Bandung, Indonesia

[2]Department of Physics, Faculty of Mathematics and Natural Science, University of Mataram, Mataram, Indonesia

[3]Research Center for Safety, Metrology and Nuclear Quality, National Research and Innovation Agency of Indonesia, Jakarta, Indonesia

freddy@itb.ac.id

ABSTRACT

The use of 3D phantoms represents patient anatomy, enabling more effective treatment planning optimization. This study aims to develop a tissue-equivalent 3D-printed phantom as a dosimetry application for the HDR-BT Cobalt-60 source. Polylactic Acid (PLA) with a single infill density of 85% was used to achieve tissue-equivalent characteristics. The phantom features a 200 mm diameter spherical structure composed of three distinct components, including an applicator channel and cavities in each layer to accommodate the HDR-BT source dose measurement detector. The characteristics of the 3D-PLA phantom were analyzed and compared with soft tissue, muscle, and water based on ICRU-44 reports, as well as with the RW3 phantom (PTW, Germany) as a standard phantom. The resulting 3D-PLA phantom density of 1.05 g/cm^3 was in good agreement with muscle, RW3 phantom, soft tissue, and water, respectively. The linear attenuation coefficient of the 3D-PLA phantom at energies >0.1 MeV and its effective atomic number (Z_{eff}) ≈ 8.26 closely resemble soft tissue properties. The HU value of the 3D-PLA phantom is –116.6 ± 7.5 HU, also within the soft tissue HU values range. These findings confirm that the developed 3D-PLA phantom exhibits the necessary characteristics for dosimetry applications.

KEYWORDS

phantom, 3D-printed, polylactic acid (PLA), HDR-brachytherapy

1 INTRODUCTION

High Dose Rate Brachytherapy (HDR-BT) using a Cobalt-60 source has become the primary choice in treatment planning due to its efficiency in delivering an optimal dose distribution [1]–[3]. Accurate quality assurance and quality control (QA/QC) procedures for HDR-BT are essential to enhance the likelihood of achieving the desired treatment outcomes, minimize the risk of errors in clinical practice, and ensure the efficacy of clinical trials [4], [5]. QA/QC tests require a suitable phantom to improve accuracy and simplify and speed up the testing process [4], [6], [7]. However, QC in HDR-BT faces significant challenges due to the limitations of available phantoms, which often do not accurately represent human tissue characteristics. In addition,

Qomariyah, N., Waris, A., Wirawan, R., Prasetio, H., Haryanto, F. (2025). Design and Development of a 3D-Printed Tissue Equivalent Phantom for Cobalt-60 HDR Brachytherapy. *International Journal of Online and Biomedical Engineering (iJOE)*, 21(9), pp. 153–168. https://doi.org/10.3991/ijoe.v21i09.55513

Article submitted 2025-03-14. Revision uploaded 2025-04-29. Final acceptance 2025-04-29.

most conventional phantoms lack flexibility in dose measurement for complex anatomy, necessitating a more adaptive approach for treatment planning validation [8], [9].

The use of phantoms is crucial for validating dose calculation algorithms and evaluating the accuracy of the treatment planning system [9], [10]. Several studies emphasized the importance of using water-equivalent phantoms in dosimetry QC. Additionally, some studies reported using polymethyl methacrylate (PMMA) and solid water phantoms in HDR-BT dosimetry studies following the TG-43 approach [11]–[15]. However, this approach has limitations in simulating actual clinical conditions, especially for reviewing tissue heterogeneity. Rivard et al. [16] revealed that although TG-43 is the standard protocol for planning and quality control of brachytherapy dosimetry, this recommendation does not fully consider the effects of heterogeneity and inhomogeneous tissue absorption.

In recent years, advancements in 3D printing have facilitated the fabrication of phantoms with complex geometric properties and tissue equivalence [5], [8], [17], [18]. Several studies have comprehensively reviewed the precision of dosimetry across various tissues through the development of 3D-printed phantoms [10], [19]. A three-dimensional phantom was developed for stereotactic radiosurgery (SRS) to facilitate patient-specific quality assurance (QA) for multiple brain targets (MBT) and to support the commissioning of complex SRS procedures. The phantom demonstrated the capability to perform MBT patient-specific QA within a single delivery [9]. Polylactic acid (PLA) is one of the most extensively developed materials for 3D phantom fabrication and has been thoroughly investigated to assess its suitability, particularly for applications in radiotherapy [17], [18], [20], [22].

This study aims to design and fabricate a 3D-printed phantom for HDR-BT sources, enabling its use for QA procedures and dose measurements within the TG-43 recommended geometry while ensuring that the phantom exhibits tissue equivalence. A previous study developed a 3D-printed phantom using PLA with an infill density of approximately ±80%, resulting in HU values within the range of human soft tissue [5]. Okkalidis et al. [17] also demonstrated that 3D-printed phantoms with varying infill densities can effectively replicate human muscle, fat, and lung tissues based on HU values derived from computed tomography (CT) images. In line with the above studies, this study focuses on developing a PLA-based 3D-printed tissue-equivalent phantom for HDR-BT source dose measurement.

Phantom characteristics for dosimetry application are designed considering geometry, radiological properties, and material composition resembling biological tissue. These characteristics are evaluated based on physical parameters, including mass density, linear attenuation coefficient, effective atomic number (Z_{eff}), and Hounsfield Unit (HU) value. These parameters represent the interaction of radiation with the material and play a role in ensuring the equivalence of the phantom to biological tissue, as the International Commission on Radiation Units and Measurements—ICRU Report 44 recommends (ICRU-44) [19], [23], [24].

2 MATERIALS AND METHODS

2.1 Design and materials of the 3D-PLA Phantom

The phantom developed in this study is a 3D-printed phantom based on polylactic acid (PLA), which is referred to as the 3D-PLA phantom. The phantom material uses PLA with a filament density of 1.24 g/cm^3. PLA is a thermoplastic polymer that is widely recognized as the most prevalent material utilized in fused deposition modelling (FDM) 3D printing applications [25]. In this study, PLA was selected due

to its biocompatibility, density, and radiation absorption properties, which closely resemble those of human tissue. Additionally, it offers ease of 3D printing, dimensional stability, and cost-effectiveness [5], [17], [26]. Furthermore, modifying the infill density can easily adjust its material density.

The 3D-PLA phantom has a spherical geometry with a diameter of 200 mm, designed following the TG-43 protocol recommendations. In the preliminary fabrication, the phantom design was developed using Tinkercad software and saved in STL file format for further fabrication processes. The 3D-PLA phantom is composed of three geometric structures: (1) a flat circular plate with a diameter of 200 mm and a thickness of 10 mm, featuring a semicylindrical channel with a 1.5 mm diameter extending from the center to the edge, serving as an applicator channel; (2) nine flat circular plates without an applicator channel, with progressively decreasing diameters forming a hemispherical structure, all maintaining a uniform thickness of 10 mm; and (3) ten bowl-shaped components, each with a thickness of 10 mm, ranging in diameter from 20 mm to a maximum of 200 mm. The applicator channel at the center of the phantom is designed to accommodate the LAA1400-GYN catheter with a diameter of 3 mm. A 0.3 mm gap between the plate layers is included to house the detector. The detailed design of the 3D-PLA phantom is illustrated in Figure 1.

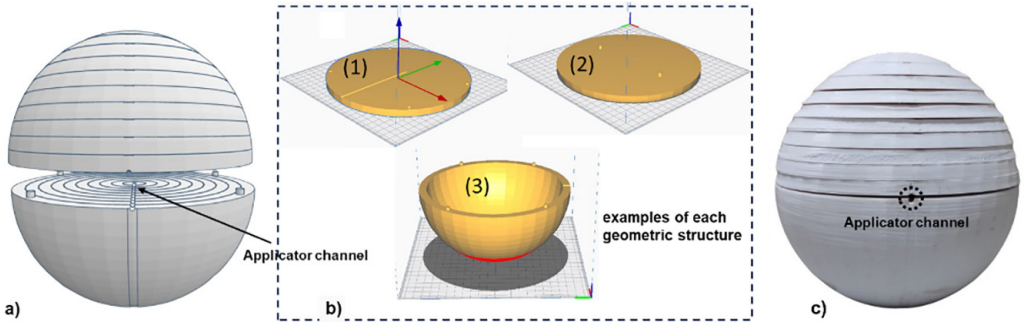

Fig. 1. a) Schematic design of the phantom with an STL file; b) examples of each geometric input for 3D printing; and c) The 3D-PLA phantom produced using a 3D printer with PLA material, featuring a diameter of 200 mm with an applicator channel of 3 mm

Figure 1a illustrates the schematic design of the phantom in STL file format. Figure 1b displays representative examples of each geometric structure (labelled (1), (2), and (3)), which function as geometric inputs for the 3D printing of the three structural elements derived from the design in Figure 1a, and the fully assembled 3D-PLA phantom is depicted in Figure 1c.

The 3D-PLA phantom features a layered design tailored for measuring dose distribution from an HDR-BT Co-60 source. Measurements include radial, horizontal, and anisotropic dose profiles. The upper section consists of ten detachable horizontal layers with varying diameters, allowing the placement of detectors (EBT3 film) at specific positions to measure radial dose and dose along the horizontal axis. This structure is optimized to ensure precise detector orientation and consistent radiation path within the medium, thereby supporting accurate verification of simulation results and experimental dosimetry measurements. Meanwhile, the lower section comprises detachable bowl-shaped layers for measuring the anisotropic dose profile.

The 3D-PLA phantom was fabricated using an Elegoo Neptune 4 Pro printer with the fused deposition modeling (FDM) technique [23], [25]–[26]. The input parameters for 3D printing are presented in Table 1. The phantom was fabricated using a single infill density of 85% to achieve the desired density of 1.05 g/cm^3, ensuring similarity to soft tissue density. An infill density of 85% was selected based on previous

studies, which demonstrated that PLA with an infill of approximately ±80% exhibits HU values and density within the range of soft tissue [5], [17], [20], [27]–[29].

Table 1. Specifications of the 3D-printing setup used for 3D-PLA phantom fabrication

Parameters	Value
Material	PLA+
Build Volume	225 × 225 × 265 mm^3
Layer Height	0.28 mm
No walls	3
Material diameter	1.75 mm
Nozzle diameter	0.4 mm
Print temperature	220 °C
Type file	.Stl
Infill	85%
Bed Temp	65 °C

2.2 Determination of 3D-PLA Phantom characteristics

The characterization of the 3D-PLA phantom was conducted by evaluating several fundamental parameters to ensure its equivalence to human tissue. According to phantom characteristics for dosimetry studies, an ideal phantom should have mass density, a linear attenuation coefficient, an effective atomic number (Z_{eff}), and uniform HU values to those of human tissue.

Mass density: The density of the 3D-PLA phantom was calculated based on the percentage of infill density value of the PLA material used. Previously, the mass densities of soft tissue, muscle, and water in the human body were studied according to ICRU-44 publications [30]. The density of the 3D-PLA phantom was determined using the following equation 1:

$$density(g/cm^3) = Infill\ density(\%) \times 1.24\ g/cm^3 \tag{1}$$

Where the infill density used is 85%, and the value of 1.24 g/cm^3 represents the density of the PLA filament. Subsequently, the density of the 3D-PLA phantom was analyzed and compared with the densities of soft tissue, muscle, and water, which had been previously studied. This analysis aimed to determine the percentage difference in density to assess the capability of the 3D-PLA phantom in simulating the physical characteristics of human tissue. The density difference between the 3D-PLA phantom and soft tissue, muscle, and water was calculated using the following equation 2:

$$\%diff = \left| \frac{\rho_{tissue} - \rho_{3D\_PLA}}{\rho_{tissue}} \right| \times 100\% \tag{2}$$

Where ρ_{tissue} represents the density of soft tissue, muscle, and water (g/cm^3) based on ICRU-44, and ρ_{3D_PLA} represents the density of the 3D-PLA phantom 3D-PLA (g/cm^3).

The effective atomic number and Linear Attenuation Coefficient: The effective atomic number (Z_{eff}) and linear attenuation coefficient of the 3D-PLA phantom are determined based on its elemental composition. This composition is critical in defining the phantom's interaction with radiation, particularly in photon absorption

and scattering processes. The elemental composition was analyzed using scanning electron microscopy (SEM) – energy dispersive X-ray (EDX) with a Jeol JCM-7000 type. The scanning process was conducted at an input voltage of 15 kV. This analysis was based on the EDX spectrum, identifying characteristic peaks corresponding to each element in the 3D-PLA phantom material.

Based on the elemental composition of the 3D-PLA phantom, soft tissue, muscle, and water were used to determine Z_{eff} using Mayneord's Formula. This method has been widely applied in various dosimetry applications and studies on radiation interactions with biological tissues. Mayneord's Formula has been proven to be a reliable approach for determining Z_{eff}, as its calculations are based on the elemental composition of a given material [31][32], using the equation 3:

$$Z_{eff} = \sqrt[p]{\sum_{i=1}^{n} w_i (Z_i)^p} \tag{3}$$

Where w_i represents the mass fraction of the *ith* element, Z_i is the atomic number of the *ith* element, and p is the exponent, with a value of 2.94 photon interactions in the medium-energy range.

Based on the elemental composition of the 3D-PLA phantom, soft tissue, muscle, and water, these components were also used to determine their respective linear attenuation coefficients. This calculation was performed using the XCOM program with elemental/compound composition. The comparison aims to assess the extent to which the 3D-PLA phantom can mimic the linear attenuation characteristics of biological tissue regarding radiation absorption [33].

Determination of Hounsfield Unit (HU) of the 3D-PLA Phantom: The determination of HU values for the 3D-PLA phantom was conducted based on CT scan imaging using a PHILIPS Brilliance CT Big Bore Scanner with a slice thickness of 2 mm. The scanning was performed under 120 kV and 316 mAs per slice. This HU value calculation aims to evaluate the uniformity of phantom density, indicating how closely the phantom structure mimics human tissue. Additionally, the uniformity of HU values across the entire phantom was analyzed to assess the homogeneity of the 3D-PLA phantom's density.

The CT scan images of the 3D-PLA phantom generated 100 slices, each with a thickness of 2 mm. The analysis of HU values in the phantom was performed using the region of interest (ROI) restriction method with the aid of DICOM viewer software. A total of 20 slices were selected for analysis, with a systematic interval of every five slices to ensure a comprehensive representation of the entire 3D-PLA phantom.

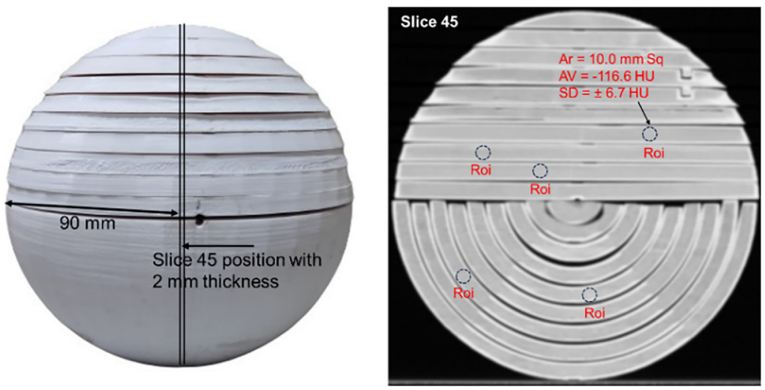

Fig. 2. Determination of Hounsfield Unit (HU) values using the Region of Interest (ROI) method on CT scan images of the 3D-PLA phantom

Hounsfield Unit values were determined for each selected slice by manually defining five ROIs at random locations, prioritizing regions with similar grayscale intensity. The ROI selection process accounted for homogeneous density regions within the phantom while excluding the wall areas, which exhibit higher density due to the structural configuration of the 3D-printing process. The ROIs were circular, with an approximate area of ±10 mm^2, shown in Figure 2. The HU values for each ROI were then calculated to obtain the average HU for each slice, which was subsequently used to determine the overall average HU of the phantom. This approach aimed to achieve a more accurate representation of the HU distribution throughout the phantom CT images.

3 RESULTS AND DISCUSSION

3.1 Characteristics of the 3D-PLA Phantom

Mass Density Analysis: The 3D-printed PLA phantom, fabricated with a uniform infill density of 85% and a PLA filament density of 1.24 g/cm^3, achieved a final density of 1.05 g/cm^3, obtained through calculations using Equation (1). The density of the 3D-PLA phantom was compared to the densities of soft tissue, muscle, and water, as reported in ICRU-44, to assess its suitability for simulating specific biological tissues. The percentage density differences between the 3D-PLA phantom and each reference are presented in Table 2. The absolute percentage differences between the 3D-PLA phantom and soft tissue, muscle, and water densities, as calculated using Equation (2), were 0.94%, 0.0%, and 5.00%, respectively. A lower percentage difference in density signifies a greater correspondence with the mass density of biological tissues. In this context, the 3D-printed PLA phantom demonstrates the highest density conformity with muscle, followed by soft tissue and water.

Table 2. Percentage difference in density between the 3D-PLA phantom and soft tissue, muscle, and water based on the ICRU-44 report

Parameters	Phantom/Human Organ			
	3D-PLA Phantom	Soft-Tissue	Muscle	Water
Mass Density (g/cm^3)	1.05	1.06	1.05	1.00
Different (%) (3D-PLA Phantom/human organ)	–	0.94	0.00	5.00

The Effective Atomic Number and Linear Attenuation Coefficient: Energy dispersive X-ray characterization reveals the spectrum of the 3D-PLA phantom with eight detected elemental peaks at an acceleration voltage of 15 kV. The elemental composition of the phantom consists of Carbon (C), Oxygen (O), Sodium (Na), Silicon (Si), Sulfur (S), Chlorine (Cl), Potassium (K), and Calcium (Ca). Carbon and Oxygen dominate the composition, comprising over 80% of the total mass, with respective mass fractions of 37.87% and 58.34%, while the other six elements exhibit minimal intensity. The comparative analysis of elemental mass composition between the 3D-PLA phantom and soft tissue, muscle, and water is presented in Table 3. Most of the identified elements are also present in biological tissues, except for hydrogen, which is absent in the 3D-PLA phantom. Based on its elemental composition, the 3D-PLA phantom is quantitatively similar to the main elements found in human organs.

Table 3. Element composition (mass percentage) of the 3D-printed phantom and the elemental composition of human organs based on the ICRU-44 report

Element Composition	3D-PLA Phantom	ICRU's Human Organ		
		Soft-Tissue	Muscle	Water
H	–	10.20%	10.20%	11.19%
C	37.87%	14.30%	14.30%	–
N	–	3.40%	3.40%	–
O	58.34%	70.80%	71.00%	88.81%
F	–	–	–	–
Na	0.97%	0.20%	0.10%	–
Si	0.59%	–	–	–
P	–	0.30%	0.20%	–
S	0.15%	0.30%	0.30%	–
Cl	0.20%	0.20%	0.10%	–
K	0.34%	0.30%	0.40%	–
Ca	1.52%	–	–	–
Fe	–	–	–	–
Z_{eff}	8.26	7.71	7.70	7.68

The effective atomic number (Z_{eff}) presented in Table 3 was determined using Mayneord's formula. The calculation results show that the Z_{eff} of the 3D-PLA phantom is 8.26, which is higher than that of soft tissue (7.71), muscle (7.70), and water (7.68). This discrepancy arises from the presence of higher atomic number elements in the 3D-PLA phantom, including silicon (Si, Z = 14), chlorine (Cl, Z = 17), potassium (K, Z = 19), and calcium (Ca, Z = 20), which collectively contribute to the increased Z_{eff}.

Based on the elemental composition listed in Table 3, the linear attenuation coefficient was obtained using the XCom software within the energy range of 30 keV to 150 keV, which is commonly used in diagnostic radiology practice [34]. The linear attenuation coefficient characterizes the interaction between radiation penetration and the absorbing medium. Figure 3 presents a comparative analysis of the linear attenuation coefficients of the 3D-PLA phantom and previously investigated biological tissues.

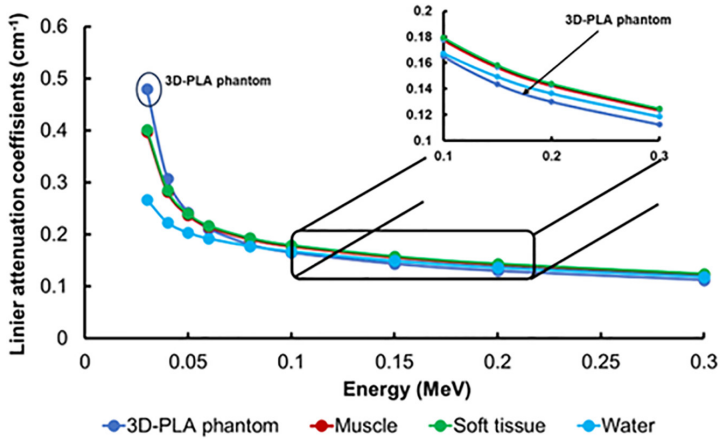

Fig. 3. Linear attenuation coefficient of the 3D-PLA phantom and human tissue (soft tissue, muscle, and water)

Based on Figure 3, the linear attenuation coefficient of the 3D-PLA phantom exhibits a similar pattern to that of soft tissue, muscle, and water. The 3D-PLA phantom shows a higher linear attenuation coefficient at low energies, whereas, at energies above 0.1 MeV, it demonstrates good agreement with soft tissue, muscle, and water. Based on elemental distribution, the PLA-based 3D-PLA phantom can replicate the linear attenuation properties of biological tissues over a broad energy range, with more noticeable differences at lower energies.

Hounsfield Unit (HU) Value: The HU values of the 3D-printed PLA phantom were extracted from a DICOM-format CT scan comprising 100 slices, each with a thickness of 2 mm. The uniform distribution of HU values indicates consistent density and structural homogeneity across the phantom. Figure 4 illustrates 20 representative CT scan slices of the 3D-PLA phantom, while Table 4 presents the distribution of HU values across these slices as analyzed using a DICOM viewer.

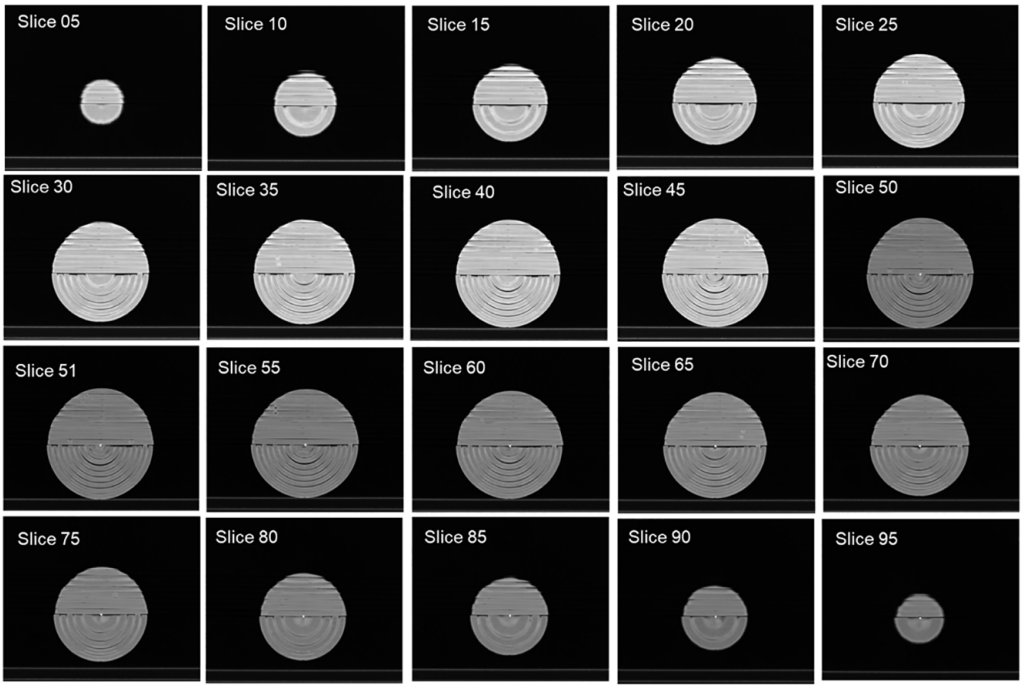

Fig. 4. CT scan images of the 3D-PLA phantom across 20 slices, taken at 5-slice intervals to represent the entire phantom image

Table 4. HU value distribution across 20 slices of the 3D-PLA phantom based on DICOM viewer

No Slice	HU Value					
	Roi 1	Roi 2	Roi 3	Roi 4	Roi 5	Mean ± SD
Slice 5	–146.1 ± 4.4	–116.5 ± 7.0	–134 ± 9.8	–130.2 ± 3.0	–110.9 ± 9.9	–127.5 ± 6.8
Slice 10	–118.8 ± 4.4	–116.3 ± 6.9	–123.8 ± 8.8	–120.7 ± 4.8	–133.8 ± 5.6	–122.7 ± 6.1
Slice 15	–123.4 ± 7.6	–136.4 ± 6.8	–126.8 ± 5.1	–113.3 ± 4.5	–126.9 ± 9.4	–125.4 ± 6.7
Slice 20	–130.6 ± 6.5	–126.3 ± 6.4	–119.8 ± 9.0	–134.0 ± 8.2	–129.1 ± 6.6	–128.0 ± 7.3
Slice 25	–116.5 ± 7.7	–115.4 ± 6.1	–120 ± 9.7	–122.7 ± 6.0	–123.8 ± 8.7	–119.7 ± 7.6
Slice 30	–126.9 ± 8.7	–121.5 ± 7.9	–121 ± 3.9	–126.3 ± 9.8	–117.1 ± 9.7	–122.6 ± 8.0

(Continued)

Table 4. HU value distribution across 20 slices of the 3D-PLA phantom based on DICOM viewer *(Continued)*

No Slice	HU Value					
	Roi 1	Roi 2	Roi 3	Roi 4	Roi 5	Mean ± SD
Slice 35	–118.7 ± 9.5	–126.9 ± 8.4	–125.7 ± 6.3	–123.4 ± 8.9	–117.0 ± 8.9	–122.3 ± 8.4
Slice 40	–103.6 ± 6.2	–106.2 ± 8.4	–100.0 ± 7.2	–105.9 ± 5.3	–123.2 ± 7.3	–107.8 ± 6.9
Slice 45	–119.7 ± 9.0	–110.0 ± 6.8	–127.9 ± 9.4	–104.8 ± 7.2	–124.2 ± 8.2	–117.32 ± 8.1
Slice 50	–105.4 ± 8.4	–123.1 ± 8.5	–109.1 ± 9.8	–133.6 ± 7.3	–107.5 ± 6.0	–115.7 ± 8.0
Slice 51	–132.9 ± 7.9	–134.7 ± 6.6	–131.1 ± 9.8	–105.0 ± 6.0	–96.8 ± 4.7	–120.1 ± 7.0
Slice 55	–131.9 ± 6.0	–98.7 ± 9.3	–131.3 ± 9.3	–113.9 ± 7.7	–104.0 ± 8.0	–116.0 ± 8.1
Slice 60	–99.2 ± 8.1	–98.1 ± 9.9	–131.3 ± 8.2	–105.4 ± 9.6	–117.1 ± 6.3	–110.2 ± 8.4
Slice 65	–96.2 ± 7.8	–107.5 ± 8.9	–129.5 ± 8.8	–107.0 ± 8.9	–135.0 ± 9.7	–115.0 ± 8.8
Slice 70	–104.0 ± 6.2	–133.2 ± 5.3	–103.5 ± 6.7	–104.0 ± 4.8	–108.0 ± 6.3	–110.5 ± 5.9
Slice 75	–128.4 ± 8.4	–102.2 ± 7.3	–114.1 ± 9.3	–102.1 ± 5.5	–128.5 ± 8.9	–115.1 ± 7.9
Slice 80	–136.8 ± 7.0	–106.2 ± 8.4	–82.8 ± 5.8	–122.7 ± 9.7	–127.2 ± 9.5	–115.1 ± 8.1
Slice 85	–127.8 ± 8.7	–140.6 ± 4.1	–92.5 ± 6.4	–82.7 ± 9.8	–95.7 ± 6.9	–107.9 ± 7.2
Slice 90	–133.9 ± 9.6	–136.0 ± 7.9	–134.9 ± 8.0	–78.1 ± 7.1	–76.3 ± 8.4	–111.8 ± 8.2
Slice 95	–133.5 ± 8.6	–87.9 ± 4.6	–133.8 ± 8.3	–74.4 ± 9.6	–78.4 ± 3.3	–101.6 ± 6.9
Mean ± SD						**116.6 ± 7.5**

Based on the ROI from 20 CT scan slices of the phantom, the average HU value of the 3D-PLA phantom was –116.6 ± 7.5 HU (refer to Table 4). This average HU value indicates that the 3D-PLA phantom is more compatible with the HU range of soft tissue than muscle and water. The outer region of the phantom exhibits higher HU values due to the increased density of the phantom walls, resulting from the 3D printing settings using the "No wall 3" option. Therefore, this outer region was excluded from determining the average HU value.

3.2 Discussion

This study uses the FDM technique to present the design and fabrication of a 3D-printed PLA phantom. The geometry and characteristics of the 3D-PLA phantom were explicitly designed for dosimetry of the HDR-BT Co-60 source. The physical characteristics of the 3D-PLA phantom were analyzed in terms of mass density, linear attenuation coefficient, Z_{eff}, and HU value. The density of the 3D-PLA phantom was 1.05 g/cm^3, equivalent to the density of muscle and soft tissue.

By applying Equation (2), the percentage density deviation of PLA filament (1.24 g/cm^3) without infill density modification was calculated. The differences obtained were up to 16.98% for soft tissue, 18.09% for muscle, and 24.00% for water. A substantial reduction in density deviation was observed when the 3D-printed PLA phantom was fabricated with an 85% infill density. The density discrepancy between 100% and 85% infill densities reached 19.00%. Therefore, adjusting the infill density in the 3D printing process is highly effective in achieving the desired phantom density [29], [34].

A comparative analysis was performed between the 3D-printed PLA phantom and standard dosimetry phantoms, such as the RW3 phantom (PTW, Freiburg, Germany). This evaluation aims to assess the compatibility of the 3D-PLA phantom with the RW3 phantom and to validate that the developed phantom meets the standard characteristics required for radiation dosimetry applications. The RW3 phantom is a standard phantom used in radiation dosimetry for dose calibration and verification in radiotherapy. The characteristics of the RW3 phantom resemble those of water and consist of the elements H, C, O, and Ti, with mass percentages of 7.59%, 90.41%, 0.80%, and 1.20%. The RW3 phantom exhibits an Z_{eff} of approximately 6.58 and a density of 1.045 g/cm^3 [7], [35], [36]. Based on the characteristics of the RW3 phantom, the 3D-PLA phantom exhibits a high degree of compatibility. The dominant element in the 3D-PLA phantom is carbon, further supporting the similarity in material properties between the two phantoms. Schneider et al. [37] identified carbon and oxygen composition as the most critical factors influencing material equivalency, primarily due to their varying water content. In this study, the fabricated 3D-PLA phantom exhibited a predominant elemental composition of carbon (37.86%) and oxygen (58.20%). Furthermore, its linear attenuation coefficient demonstrated strong agreement with that of soft tissue, muscle, and water (Figure 3).

Although the RW3 phantom is commonly used in external radiotherapy dosimetry, it has limitations when applied to brachytherapy studies. One of the limitations of the RW3 phantom is its inability to accurately replicate secondary scattering effects within the patient, potentially impacting dose calculation precision. Furthermore, as a solid and homogeneous material, the RW3 phantom is less capable of simulating tissue heterogeneity, such as bone and air cavities. Its limitations in accommodating applicators or radioactive sources make it less ideal for verifying dose distribution in brachytherapy applications. Due to these limitations, water-equivalent or synthetic soft tissue phantoms are commonly favored in brachytherapy studies to represent clinical conditions accurately. In contrast, the 3D-PLA phantom ($Z_{eff} \approx 8.26$) exhibits more significant similarity to soft tissue properties than PMMA ($Z_{eff} \approx 6.49$), making it a more suitable candidate for phantoms in dosimetry applications.

In calibration and validation of dosimetry systems, conventional phantoms such as PMMA, solid water, and RW3 remain the standard due to their homogeneous composition and radiation attenuation characteristics, which closely approximate human tissue [38], [39]. However, their limited ability to replicate complex anatomical structures and low flexibility pose challenges in specific applications. To overcome these limitations, 3D-printing technology has been introduced as a promising alternative, enabling the fabrication of phantoms with intricate geometries tailored to specific clinical requirements [5], [24], [26]. Among the various materials employed for tissue-equivalent phantom construction, PLA has gained significant attention and is further explored in this study. Despite enhancing geometric flexibility, challenges persist, particularly regarding radiological property mismatches and density variations arising from the printing process. Therefore, selecting appropriate phantom materials for dosimetry applications requires carefully evaluating their advantages and limitations to ensure precise radiation dose measurements. Table 5 presents a comparative analysis of the physical properties of the 3D-PLA phantom, water, and standard phantoms frequently utilized in dosimetry research.

Table 5. Physical properties of the 3D-PLA phantom, PLA, water, and standard phantoms used in dosimetry

References	Materials	Density (g/cm³)	Zeff	Chemical Composition (Percentage by Mass)						
				H	C	N	O	Ca	Ti	Etc
This study	3D-PLA	1.05	8.26	–	37.87	–	58.34	1.52	–	2.27
[35]	RW3	1.045		7.59	90.41	–	0.80	–	1.20	–
[36]	RW3	–	6.58	–	–	–	–	–	–	–
[40]	PLA	1.25	–	5.29	51.86	–	42.61	–	–	0.23
[41]	Water	0.998	7.42	11.2	–		–	88.8	–	–
	Solid water	1.015	7.29	8.1	67.2	2.4	19.9	2.3		0.1
	PMMA	1.19	6.096	8.1	60.0		32.0	–	–	–

The application of PLA filament utilizing the FDM printing technique is highly recommended for the fabrication of radiotherapy dosimetry phantoms, as it minimizes geometric errors and demonstrates a high level of compatibility with standard dosimetry phantoms [19], [23]. The primary factor in the fabrication of tissue-equivalent dosimetry phantoms using 3D printing is the infill density of the filament used [20], [28], [29]. The precise selection of infill density is a critical factor in determining the characteristics of the dosimetry phantom, including HU values, attenuation coefficient, and Z_{eff}. The study by [19] reported a correlation between infill density and the resulting phantom density across different 3D printing materials. Their study indicated that a 90% infill density setting for a PLA filament (1.23 g/cm³) produced an average density of 1.04 g/cm³, demonstrating its potential for application in patient-specific phantom development [19]. This value is slightly lower than the results of this study, which demonstrated a density of 1.05 g/cm³ for PLA filament with a density of 1.24 g/cm³ and an infill density of 85%.

A 3D-printed Rando phantom was developed using PLA powder and plaster, revealing a strong correlation between infill density and Hounsfield Unit (HU) values, with a determination coefficient (R^2) of 0.999. Their findings indicated lower infill densities resulted in more significant structural non-uniformity within the phantom, whereas higher infill densities improved homogeneity. Furthermore, soft tissue equivalence was achieved with an HU value of –20 by employing an infill density of 82% [5]. Several studies investigated the influence of infill density on the HU values of PLA-based materials [20], [24]. Oh et al. [20] reporting HU values of –130 at an infill density of 85%. A comparable study investigating the influence of infill density on the HU values of PLA-based phantoms reported an HU value of –161.24 for a 3D-printed phantom fabricated using the conventional FDM technique with an infill density of 85% [17]. This study demonstrated a good agreement in HU values, with an average HU of –116.6 ± 7.5 HU using an infill density of 85%.

Several factors contribute to differences in the characteristics of the resulting phantom, even when the same type of material is used. These factors include the printing method, printer type, and manufacturer-specific material characteristics [17], [23]. Meanwhile, the primary factor to consider in fabricating tissue-equivalent phantoms using 3D printing is the infill density of the filament [19], [23]. Additionally, parameters such as extrusion rate and temperature control enable the printing of objects with more precise physical characteristics to meet specific application needs [20], [22], [42]. The 3D-PLA phantom developed in this study demonstrates its

suitability as a phantom for dosimetry studies and its potential for application in QA for HDR brachytherapy sources.

4 CONCLUSION

The 3D-PLA phantom with an 85% infill density exhibits strong potential as a dosimetry phantom for brachytherapy source applications. Characterization results indicate a density of 1.05 g/cm^3, an average HU of –116.6 ± 7.5 HU, and a linear attenuation coefficient comparable to that of water, with a $Z_{eff} \approx 8.26$), generally indicating good compatibility with soft tissue. Another advantage of the 3D-PLA phantom is its flexible geometric design, allowing for dose distribution measurements for brachytherapy sources. The results of this study indicate that the 3D-PLA phantom is suitable as an alternative soft tissue phantom for brachytherapy dosimetry and can be effectively applied in dosimetry QA for both treatment planning and clinical verification in High Dose Rate Brachytherapy (HDR-BT).

5 ACKNOWLEDGEMENTS

The authors are grateful to the Center for Higher Education Funding and Assessment (PPAPT) of the Ministry of Higher Education, Science, and Technology of Republic Indonesia, Education Fund Management Institute (LPDP), and the Indonesian Education Scholarship (BPI) for the funding support for doctoral studies.

6 REFERENCES

[1] J. F. Almansa, R. Guerrero, J. Torres, and A. M. Lallena, "Monte Carlo dosimetric characterization of the Flexisource Co-60 high-dose-rate brachytherapy source using PENELOPE," *Brachytherapy*, vol. 16, no. 5, pp. 1073–1080, 2017. https://doi.org/10.1016/j.brachy.2017.04.245

[2] I. M. Anwarul, M. M. Akramuzzaman, and G. A. Zakaria, "EGSnrc Monte Carlo-aided dosimetric studies of the new BEBIG 60Co HDR brachytherapy source," *J. Contemp. Brachytherapy*, vol. 5, no. 3, pp. 148–156, 2013. https://doi.org/10.5114/jcb.2013.37419

[3] I. Fotina, K. Zourari, V. Lahanas, E. Pantelis, and P. Papagiannis, "A comparative assessment of inhomogeneity and finite patient dimension effects in 60Co and 192Ir high-dose-rate brachytherapy," *J. Contemp. Brachytherapy*, vol. 10, no. 1, pp. 73–84, 2018. https://doi.org/10.5114/jcb.2018.74327

[4] P. Pittet *et al.*, "DoRGaN: Development of quality assurance and quality control systems for high dose rate brachytherapy based on GaN dosimetry probes," *IRBM*, vol. 39, no. 4, pp. 279–290, 2018. https://doi.org/10.1016/j.irbm.2018.04.005

[5] S. Y. Kim, J. W. Park, J. Park, J. W. Yea, and S. A. Oh, "Fabrication of 3D printed head phantom using plaster mixed with polylactic acid powder for patient – specific QA in intensity-modulated radiotherapy," *Sci. Rep.*, vol. 12, p. 17500, 2022. https://doi.org/10.1038/s41598-022-22520-6

[6] M. Arjunan, S. C. Sekaran, B. Sarkar, and S. Manikandan, "A homogeneous water-equivalent anthropomorphic phantom for dosimetric verification of radiotherapy plans," *Journal of Medical Physics*, vol. 43, no. 2, pp. 100–105, 2018. https://doi.org/10.4103/jmp.JMP_123_17

[7] A. A. Schoenfeld *et al.*, "Water equivalent phantom materials for 192Ir brachytherapy," *Phys. Med. Biol.*, vol. 60, p. 9403, 2015. https://doi.org/10.1088/0031-9155/60/24/9403

[8] S. Kang *et al.*, "Development of dosimetric verification system for patient-specific quality assurance of high-dose-rate brachytherapy," *Front. Oncol.*, vol. 11, p. 647222, 2021. https://doi.org/10.3389/fonc.2021.647222

[9] G. Mukwada *et al.*, "Development of a 3D printed phantom for commissioning and quality assurance of multiple brain targets stereotactic radiosurgery," *Phys. Eng. Sci. Med.*, vol. 47, pp. 455–463, 2024. https://doi.org/10.1007/s13246-023-01374-w

[10] A. Kanani, A. Owrangi, M. Yazdi, A. Fatemi-ardekani, and M. A. Mosleh-shirazi, "Development of a multi-purpose quality control phantom for MRI-based treatment planning in high-dose-rate brachytherapy of cervical cancer," *Journal of Contemporary Brachytherapy,* vol. 15, no. 1, pp. 57–68, 2023. https://doi.org/10.5114/jcb.2023.125014

[11] N. S. Ab Shukor, M. Musarudin, R. Abdullah, and M. Z. Abd Aziz, "Effects of different volumes of inhomogeneous medium to the radial dose and anisotropy functions in HDR brachytherapy," *Journal of Physics: Conference Series*, vol. 1497, p. 012027, 2020. https://doi.org/10.1088/1742-6596/1497/1/012027

[12] S. C. Uniyal, U. C. Naithani, and S. D. Sharma, "Evaluation of Gafchromic EBT2 film for the measurement of anisotropy function for high-dose-rate 192Ir brachytherapy source with respect to thermoluminescent dosimetry," *Reports of Practical Oncology and Radiotherapy*, vol. 16, no. 1, pp. 14–20, 2011. https://doi.org/10.1016/j.rpor.2010.11.003

[13] J. L. Reed *et al.*, "Experimental and Monte Carlo dosimetric characterization of a 1 cm 103 Pd brachytherapy source," *Brachytherapy*, vol. 13, no. 6, pp. 657–667, 2014. https://doi.org/10.1016/j.brachy.2014.04.001

[14] J. M. Geraldo *et al.*, "Monte Carlo simulation and dosimetry measurements of an experimental approach for in vitro HDR brachytherapy irradiation," *Applied Radiation and Isotopes*, vol. 172, p. 109666, 2021. https://doi.org/10.1016/j.apradiso.2021.109666

[15] A. Moutsatsos *et al.*, "Experimental determination of the Task Group-43 dosimetric parameters of the new I25.S17plus ^{125} I brachytherapy source," *Brachytherapy*, vol. 13, no. 6, pp. 618–626, 2014. https://doi.org/10.1016/j.brachy.2014.07.001

[16] M. J. Rivard *et al.*, "Update of AAPM Task Group No. 43 Report: A revised AAPM protocol for brachytherapy dose calculations," *Medical Physics*, vol. 31, no. 3, pp. 633–674, 2004. https://doi.org/10.1118/1.1646040

[17] N. Okkalidis, C. Chatzigeorgiou, and D. Okkalides, "Assessment of 11 available materials with custom three- dimensional-printing patterns for the simulation of muscle, fat, and lung hounsfield units in patient-specific phantoms," *Journal of Medical Diagnostics*, vol. 1, no. 1, p. 011003, 2018. https://doi.org/10.1115/1.4038228

[18] D. Provenzano, H. Aghdam, S. Goyal, M. Loew, and Y. J. Rao, "3D-printing in radiation oncology : Development and validation of custom 3D-printed brachytherapy alignment device and phantom," *bioRxiv*, 2022. https://doi.org/10.1101/2022.07.03.498548

[19] M. M. Mille, K. T. Griffin, R. Maass-Moreno, and C. Lee, "Fabrication of a pediatric torso phantom with multiple tissues represented using a dual nozzle thermoplastic 3D printer," *Journal of Applied Clinical Medical Physics*, vol. 21, no. 11, pp. 226–236, 2020. https://doi.org/10.1002/acm2.13064

[20] S. A. Oh *et al.*, "Feasibility of fabricating variable density phantoms using 3D printing for Quality Assurance (QA) in radiotherapy," *Progress in Medical Physics*, vol. 28, no. 3, pp. 106–110, 2017. https://doi.org/10.14316/pmp.2017.28.3.106

[21] M. Bellezzo *et al.*, "Advanced design, simulation, and dosimetry of a novel rectal applicator for contact brachytherapy with a conventional HDR 192Ir source," *Brachytherapy*, vol. 19, no. 4, pp. 544–553, 2020. https://doi.org/10.1016/j.brachy.2020.03.009

[22] S. Crowe *et al.*, "Use of light-weight foaming polylactic acid as a lung-equivalent material in 3D printed phantoms," *Phy. Eng. Sci. Med.*, vol. 46, pp. 1811–1817, 2023. https://doi.org/10.1007/s13246-023-01318-4

[23] T. Kamomae *et al.*, "Physica Medica Three-dimensional printer-generated patient-specific phantom for artificial in vivo dosimetry in radiotherapy quality assurance," *Physica Medica: European Journal of Medical Physics*, vol. 44, pp. 205–211, 2017. https://doi.org/10.1016/j.ejmp.2017.10.005

[24] Y. Choi, Y. J. Jang, K. B. Kim, J. Bahng, and S. H. Choi, "Characterization of tissue equivalent materials using 3D printing for patient-specific DQA in radiation therapy," *Appl. Sci.*, vol. 12, no. 19, p. 9768, 2022. https://doi.org/10.3390/app12199768

[25] A. Aljazara *et al.*, "Quality of 3D printed objects using Fused Deposition Modeling (FDM) technology in terms of dimensional accuracy," *International Journal of Online and Biomedical Engineering (iJOE)*, vol. 19, no. 14, pp. 45–62, 2023. https://doi.org/10.3991/ijoe.v19i14.43761

[26] T. Kairn *et al.*, "Quasi-simultaneous 3D printing of muscle-, lung- and bone-equivalent media: A proof-of-concept study," *Phys. Eng. Sci. Med.*, vol. 43, pp. 701–710, 2020. https://doi.org/10.1007/s13246-020-00864-5

[27] T. van Wagenberg *et al.*, "Treatment verification in high dose rate brachytherapy using a realistic 3D printed head phantom and an imaging panel," *Brachytherapy*, vol. 22, no. 2, pp. 269–278, 2023. https://doi.org/10.1016/j.brachy.2022.11.012

[28] S. Park, N. Choi, B. G. Choi, D. M. Lee, and N. Y. Jang, "Radiological characteristics of materials used in 3-dimensional printing with various infill densities," *Progress Medical Physics*, vol. 30, no. 4, pp. 155–159, 2019. https://doi.org/10.14316/pmp.2019.30.4.155

[29] A. P. Hariyanto, K. H. Christianti, A. Rubiyanto, N. Nasori, M. Haekal, and E. Endarko, "The effect of pattern and infill percentage in 3D printer for phantom radiation applications," *Jurnal ILMU DASAR*, vol. 23, no. 2, pp. 87–92, 2022. https://doi.org/10.19184/jid.v23i2.27256

[30] ICRU, "Tissue substitutes in radiation dosimetry and measurement," Report 44. International Commission on Radiation Units and Measurements, Maryland, USA, 1989.

[31] T. Liu, G. Hong, and W. Cai, "A comparative study of effective atomic number calculations for dual-energy CT," *Medical Physics*, vol. 48, no. 10, pp. 5908–5923, 2021. https://doi.org/10.1002/mp.15166

[32] I. Kanno, Y. Yamashita, M. Kimura, and F. Inoue, "Nuclear instruments and methods in physics research a effective atomic number measurement with energy-resolved X-ray computed tomography," *Nucl. Inst. Methods Phys. Res. A*, vol. 787, pp. 121–124, 2015. https://doi.org/10.1016/j.nima.2014.11.072

[33] J. Mason, B. Al-Qaisieh, P. Bownes, A. Henry, and D. Thwaites, "Investigation of interseed attenuation and tissue composition effects in 125I seed implant prostate brachytherapy," *Brachytherapy*, vol. 13, no. 6, pp. 603–610, 2014. https://doi.org/10.1016/j.brachy.2014.04.004

[34] M. M. Alssabbagh, A. A. Tajuddin, M. A. Manap, and A. Medical, "Evaluation of nine 3D printing materials as tissue equivalent materials in terms of mass attenuation coefficient and mass density," *International Journal of Advanced and Applied Sciences*, vol. 4, no. 9, pp. 168–173, 2017. https://doi.org/10.21833/ijaas.2017.09.024

[35] M. Cameron, D. Cutajar, and J. Davis, "Comparison of phantom materials for use in quality assurance of microbeam radiation therapy," *J. Synchrotron Rad*, vol. 24, pp. 866–876, 2017. https://doi.org/10.1107/S1600577517005641

[36] M. Kurudirek, "Water equivalence study of some phantoms based on effective photon energy, effective atomic numbers and electron densities for clinical MV X-ray and Co-60 γ-ray beams," *Nucl. Instruments Methods Phys. Res. Sect. A Accel. Spectrometers, Detect. Assoc. Equip.*, vol. 701, no. 11, pp. 268–272, 2013. https://doi.org/10.1016/j.nima.2012.10.076

[37] W. Schneider, T. Bortfeld, and W. Schlegel, "Correlation between CT numbers and tissue parameters needed for Monte Carlo simulations of clinical dose distributions," *Phys. Med. Biol.*, vol. 45, p. 459, 2000. https://doi.org/10.1088/0031-9155/45/2/314

[38] V. Lohrabian, A. Kamali-Asl, H. Arabi, H. Hemmati, and M. P. Esfahani, "Dosimetric characterization of a new 192 Ir pulse dose rate brachytherapy source with the Monte Carlo simulation and thermoluminescent dosimeter," *arXiv preprint arXiv:2102.05953*, 2021. [Online]. Available: https://arxiv.org/abs/2102.05953

[39] N. S. Ab Shukor, M. Musarudin, R. Abdullah, and M. Z. Abdul Aziz, "Dose distribution of 192Ir HDR brachytherapy source measurement using Gafchromic® EBT3 film dosimeter and TLD-100H," *Pertanika Journal if Science and Technology*, vol. 30, no. 1, 2022. https://doi.org/10.47836/pjst.30.1.37

[40] M. Alssabbagh, A. A. Tajuddin, M. A. Manap, and R. Zainon, "Author's accepted manuscript," *Radiat. Phys. Chem.*, vol. 135, pp. 106–112, 2017. https://doi.org/10.1016/j.radphyschem.2017.02.009

[41] S. Sahoo, T. P. Selvam, R. S. Vishwakarma, and G. Chourasiya, "Monte Carlo modeling of 60 Co HDR brachytherapy source in water and in different solid water phantom materials," *Journal of Medical Physics*, vol. 35, no. 1, pp. 15–22, 2010. https://doi.org/10.4103/0971-6203.58779

[42] R. Y. Kim, S. R. Marcrom, and S. Shen, "Selection of brachytherapy applicators based on tumor size and shape for cervical cancer: Simulation analysis of pear-shaped isodose dimensions," *Med. Dosim.*, vol. 46, no. 4, pp. 431–434, 2021. https://doi.org/10.1016/j.meddos.2021.06.002

7 AUTHORS

Nurul Qomariyah is a doctoral student at the Faculty of Mathematics and Natural Sciences, Institut Teknologi Bandung, Indonesia. She specializes in medical physics, with particular interest in the development and implementation of Monte Carlo-based methods for radiation therapy. Her work aims to enhance the accuracy and efficacy of radiotherapy treatments through computational modeling (E-mail: nurulqomariyah@unram.ac.id).

Abdul Waris is a Professor at the Faculty of Mathematics and Natural Sciences, Institut Teknologi Bandung, Indonesia. He specializes in the research and development of fourth-generation nuclear reactor designs, particularly the Molten Salt Reactor (MSR), and conducts studies related to reactor safety, efficiency, and nuclear safety systems using computational simulations. He is also actively involved in various national projects and international collaborations to support the advancement of safe and efficient nuclear energy technologies in Indonesia (E-mail: awaris@fi.itb.ac.id).

Rahadi Wirawan is an Associate Professor at the Faculty of Mathematics and Natural Sciences, University of Mataram, Indonesia. His research encompasses radiation physics and instrumentation, with a particular focus on radiation simulation for radiation protection and the development of microcontroller-based detection devices (E-mail: rwirawan@unram.ac.id).

Heru Prasetio is a senior researcher in medical physics and radiation protection at the Research Center for Safety, Metrology, and Nuclear Quality, National Research and Innovation Agency of Indonesia (BRIN). His research focuses on medical physics, radiation protection, dosimetric systems, and the assessment of public exposure to natural radiation sources. He has contributed to studies on radiation dosimetry in medicine and public exposure to radon and thoron. Additionally, he is involved

in national standardization efforts to enhance the safety of nuclear applications in Indonesia (Email: heru014@brin.go.id).

Freddy Haryanto is an Associate Professor at the Faculty of Mathematics and Natural Sciences, Institut Teknologi Bandung, Indonesia. His primary research expertise is in medical physics, with a particular focus on utilizing Monte Carlo simulations to enhance radiation therapy and diagnostic imaging techniques. Committed to advancing medical science, he specializes in developing and applying innovative physics-based methodologies to improve healthcare outcomes (E-mail: freddy@itb.ac.id).